

ATOMISTIC INVESTIGATIONS OF THE THERMODYNAMICAL STABILITY AND MARTENSITIC NUCLEATION OF $\text{Fe}_{80}\text{Ni}_{20}$ NANOPARTICLES

K. KADAU *and P. ENTEL

*Theoretische Tieftemperaturphysik,
Gerhard-Mercator-Universität, 47048 Duisburg, Germany*

(Received ...)

Abstract

The study of the thermodynamical stability of $\text{Fe}_{80}\text{Ni}_{20}$ nanoparticles in the framework of embedded-atom method and molecular-dynamics simulations shows evidence of large surface contributions to the free energy for particles with diameters up to 15 nm or more. The change of the free energy compared to its bulk value leads to a reduction of the martensitic equilibrium temperature, M_0 , and can suppress martensitic transformations in small particles. In addition the formation of martensite can be suppressed due to the lack of pre-existing nucleation sites necessary to overcome the energy barrier along the transformation path from austenite to martensite.

Keywords: Fe–Ni nanoparticles, Martensitic transformation, Molecular-dynamics simulations

1. INTRODUCTION

Early experimental investigations by Cech and Turnbull (1957) of Fe-Ni alloy powder showed a reduction of the martensitic transformation temperature, M_s , or even the suppression of the transformation in particles of some 10 μm in diameter (Wayman and Bhadeshia, 1996; Delaey, 1991). They interpreted

*Corresponding author, tel. +49-203-3792794, fax: +49-203-3793665, email: kai@thp.uni-duisburg.de

this effect as to be due to the lack of heterogeneities and other nucleation sites in the small particles, so that heterogeneous nucleation of martensite could not take place. Since experimental techniques have been refined with time, the investigation of smaller particles with diameters in the nm range is now possible. For example, Tadaki *et al.* (1996) investigated nanoparticles of Fe-Ni alloys with a diameter around 6 nm, i.e. particles with ca. 10^3 atoms. They found a reduction of the martensitic start temperature, M_s . Their explanation is that the equilibrium temperature M_0 (corresponding to equal free energies of martensite and austenite) is reduced with decreasing particle size. Here we report estimations of the surface energy of martensitic and austenitic nanoparticles based on embedded-atom method (EAM) (Daw and Baskes, 1984) calculations. In addition, nucleation processes at pre-existing defects of particles up to 24 nm diameter have been studied by molecular-dynamics (MD) simulations. The results are discussed in view of the free-energy barriers along the transformation path between the austenite and martensite structure (i.e. fcc and bcc).

2. COMPUTATIONAL

The application of the EAM model to Fe and Ni developed by Meyer and Entel (1998) has yielded reasonable results for the martensitic and austenitic transition in bulk systems (Entel, Kadau, Meyer, Herper *et al.*, 1998) and in thin films (Kadau, Meyer and Entel, 1999). We have used standard MD, as described, for example, by Rapaport (1995), and the same EAM model to study nucleation in nanoparticles. For the large-scale simulations we used the SPaSM code developed by the Los Alamos group (Lomdahl, Tamayo, Jensen and Baezley, 1993; Baezley and Lomdahl, 1997). For the evaluation of free-energy differences we used the total differential of the free energy $F(T, V)$ (Landau and Lifshitz, 1993),

$$dF = -PdV - SdT, \quad (1)$$

where P is the pressure, V the volume, S the entropy, and T is the temperature of the system. Using Cartesian components the free energy can be written as (for simulations at constant temperature)

$$dF = -P_{xx}A_{yz}dx - P_{yy}A_{zx}dy - P_{zz}A_{xy}dz, \quad (2)$$

with P_{ii} the pressure components along the three Cartesian axes and A_{jk} the respective perpendicular cross sections (Allen and Tildesley, 1987).

3. RESULTS AND DISCUSSION

In order to estimate the influence of surface energies of martensite and austenite particles, we considered first elemental iron. A useful quantity which can

be obtained from the binding (see Table 1) and surface energies (see Table 2), is the ratio of the difference of surface energies for the fcc and bcc structures to the difference of bulk energies for fcc and bcc as a function of particle diameter d (d is measured in units of the lattice constant of the bcc structure, a_{bcc}). For example, for Fe we obtain for a fixed temperature ($T = 100$ K) the following scaling behavior,

$$\left(\frac{\Delta E_{\text{surf}}^{\text{fcc-bcc}}}{\Delta E_{\text{bulk}}^{\text{fcc-bcc}}} \right)_{T=100 \text{ K}} \approx 5/d. \quad (3)$$

The calculation was done by assuming that half of the surface of the austenitic particle consists of fcc(100), the other half of fcc(111), while for the martensitic particle half of the surface was taken to be bcc(100), the other half bcc(110). The formula exhibits crossover behavior: For $d < 5 a_{\text{bcc}}$ the surface contribution to the energy difference between the martensitic- and austenitic-particle dominates over the bulk contribution, whereas for particle diameters $d \approx 50$ the surface contribution has decreased to 10%.

Since the surface favors the fcc structure, i.e. austenite (see Table 2), one would expect that the martensitic structure of small particles becomes thermodynamically unstable. In order to check this we prepared ideal spheres of bcc packed $\text{Fe}_{80}\text{Ni}_{20}$ material and performed MD runs from 25 K up to 700 K in steps of 25 K for 17.52 ps (corresponding to 12.000 time steps of 1.46 fs). As result we find that the smaller the particle the more unstable becomes the bcc structure upon heating. Table 3 contains the austenitic transformation temperatures, A , for $\text{Fe}_{80}\text{Ni}_{20}$ nanoparticles of different sizes. Due to the absence of intrinsic defects in the particles (apart from vacancies in the nearly spherical surface) and due to the small system sizes the austenite start, A_s , and austenite final, A_f , temperatures are identical. Ultra-small particles with diameters less than 10 bcc lattice constants are not stable at all in the bcc structure. For such small system sizes the atoms near the surface transform at very low temperatures into a closed-packed structure, whereas the core of the particle still exhibits the bcc structure. For temperatures $T \approx A$ also the core transforms into the austenitic structure. A plot of A versus $1/d$ shows a linear increase with increasing d , whereby the linear scaling extends up to the bulk value of A (this holds also for elemental iron, which shows that with respect to the nature of structural transformations, the element does not behave differently compared to its alloy analogues). A breakdown of the scaling is expected to occur for very small particles, however, this has not been investigated in detail.

A similar scaling is not observed for the reverse transformation from the fcc phase to the martensitic bcc structure with decreasing temperature. In fact, for defect-free particles we do not observe the reverse transformation at all. The experimental martensite start, M_s , and martensite final, M_f , temperatures occur in the magnetic alloys at much lower temperatures compared to A_s and A_f , at least for a concentration of Ni atoms beyond its percolation threshold, see Fig. 1 in Schröter *et al.* (1995). Obviously the

martensitic transformation at the lower temperatures require the presence of intrinsic defects, which has been confirmed in the simulations for Fe-Ni bulk alloys, where the transformation can be induced, for example, by a sufficient amount of vacancies (a systematic study of different kinds of defects has yet to be undertaken). This can be explained by the observation that the austenitic transformation with increasing T is an entropy driven transformation, whereas during the transformation with decreasing T the alloy has difficulties of reducing the excess entropy of the high-temperature phase (see the discussion of the free energy below). The simulations of a perfectly spherical fcc $\text{Fe}_{80}\text{Ni}_{20}$ nanoparticle containing about half a million atoms at $T = 50$ K has shown that the fcc structure remains meta-stable. Introducing defects like a missing half plane, allows the particle to transform into the thermodynamically stable bcc structure. The corresponding heterogeneous nucleation process is shown in Fig. 1. Figure 2 shows the time evolution of the radial distribution function of the particle. The transformation from fcc to bcc is accompanied by a splitting of the first nearest-neighbor peak of the fcc distribution function.

As mentioned a systematic study of the influence of various defects on $A_{s,f}$ and $M_{s,f}$ has still to be done. Also systematic experimental investigations cannot be found in the literature. A few investigations were done for the non-magnetic Cu-Zn and Cu-Zn-Al alloys, where, however, in contrast to the magnetic alloys the hysteresis between transformation and retransformation is small, being only of a few degrees (Ahlers, 1986). Nevertheless, the M_s temperatures from polycrystalline materials can be quite different from those of single crystals. In addition, since many of alike shape-memory alloys are annealed at high temperatures in order to homogenize them, before quenching them into water, M_s also depends on the annealing procedure. This makes it difficult to discuss thermodynamic properties of martensites in a unified manner.

With respect to the Fe-Ni alloys we can obtain a hint why the austenite transformation might be different from the corresponding martensite one. Figure 3 shows the behavior of the free energy along the Bain path between the bcc and fcc phase for different temperatures. For high temperatures we find a single minimum corresponding to the austenite phase, whereas at low-temperatures the free-energy curve exhibits two minima separated by a small energy barrier. This shows that the nucleation of martensite requires pre-existing defects which can locally reduce the energy barrier and initiate the heterogeneous nucleation process.

Acknowledgements

This work was supported by the DFG-Graduiertenkolleg *Struktur und Dynamik heterogener Systeme* and the SFB 445. It is a pleasure to thank T. C. Germann, P. S. Lomdahl, and B. L. Holian from Los Alamos for many

helpful discussion and for the SPaSM code.

References

- Ahlers, M. (1986). Martensite and equilibrium phases in Cu-Zn and Cu-Zn-Al phases. *Progr. Mater. Sci.*, **30**, 135.
- Allen, M. P. and D. J. Tildesley (1987). *Computer Simulation of Liquids*. Clarendon Press, Oxford.
- Beazley, D. M. and P. S. Lomdahl (1997). Controlling the data glut in large-scale molecular-dynamics simulations. *Computers in Physics*, **11**, 230.
- Cech, R. E. and D. Turnbull (1957). Heterogeneous nucleation of the martensite transformation. *Trans. AIME*, **206**, 124.
- Daw, M. S. and M. I. Baskes (1984). Embedded-atom method: Derivation and application to impurities, surfaces, and other defects in metals. *Phys. Rev. B* **29**, 6443.
- Delaey, L. (1991). Diffusionless transformations. In R. W. Cahn, P. Haasen and E. J. Kramer, editors, *Phase Transformations in Materials*, volume 5 of *Materials Science and Technology*, 339. VCH, Weinheim.
- Entel, P., K. Kadau, R. Meyer, H. C. Herper *et al.* (1998). Large-scale molecular-dynamics simulations of martensitic nucleation and shape-memory effects in transition metal alloys. *Phase Transitions*, **65**, 79.
- Kadau, K., R. Meyer and P. Entel (1999). Molecular-dynamics study of thin iron films on copper. *Surf. Rev. Lett.*, **6**, 35.
- Landau, L. D. and E. M. Lifshitz (1993). *Statistical Physics*. Pergamon Press, Oxford.
- Lomdahl, P. S., P. Tamayo, N. G. Jensen and D. M. Baezley (1993). 50 gflops molecular dynamics on the connection machine 5. In G. S. Ansell, editor, *Proceedings of Supercomputing '93*, 520. IEEE Computer Society Press.
- Meyer, R. and P. Entel (1998). Martensite-austenite transition and phonon dispersion curves of $\text{Fe}_{1-x}\text{Ni}_x$ studied by molecular-dynamics simulations. *Phys. Rev. B*, **57**, 5140.
- Rapaport, D. C. (1995). *The Art of Molecular Dynamics Simulation*. Cambridge University Press, Cambridge.
- Schröter, M., H. Ebert, H. Akai, P. Entel *et al.* (1995). First-principles investigations of atomic disorder effects on magnetic and structural instabilities in transition metal alloys. *Phys. Rev. B*, **52**, 188.
- Tadaki, T., Y. Murai, A. Koreeda, Y. Nakata *et al.* (1996). Structure and phase transformation of nano-scale particles of Fe-Ni alloys. *Mater. Sci. and Engineer. A*, **217/118**, 235.

Wayman, C. M. and H. K. D. H. Bhadeshia (1996). Phase transformations, non-diffusive. In R. W. Cahn and P. Haasen, editors, *Physical Metallurgy*, volume 2, chapter 16. North-Holland, Amsterdam.

Table 1: Binding energies in Ry obtained for bulk Fe with the EAM potentials for different structures and temperatures.

Structure	100 K	300 K
bcc Fe	0.31363	0.31173
fcc Fe	0.31085	0.30945

Table 2: Surface energies in units of 10^{-3} Ryd/ a_{Bohr}^2 obtained with the EAM potentials for Fe. Surface energies of bcc(100) and bcc(110) are larger than corresponding surface energies of fcc(100) and fcc(111), respectively. The surface energies for Fe₈₀Ni₂₀ alloys are very similar, especially with respect to differences of energies.

Surface	100 K	300 K
bcc (100)	2.2457	2.2954
bcc (110)	1.8041	1.8384
fcc (100)	2.0000	2.0086
fcc (111)	1.7250	1.7314

Table 3: Transition temperatures for the martensite to austenite transformation in Fe₈₀Ni₂₀ nanoparticles. d is the diameter (in multiples of a_{bcc}), N is the number of atoms and A the austenitic transition temperature in K.

d	N	A
8	544	250
10	1056	350
15	3582	425
20	8388	500
30	28276	550

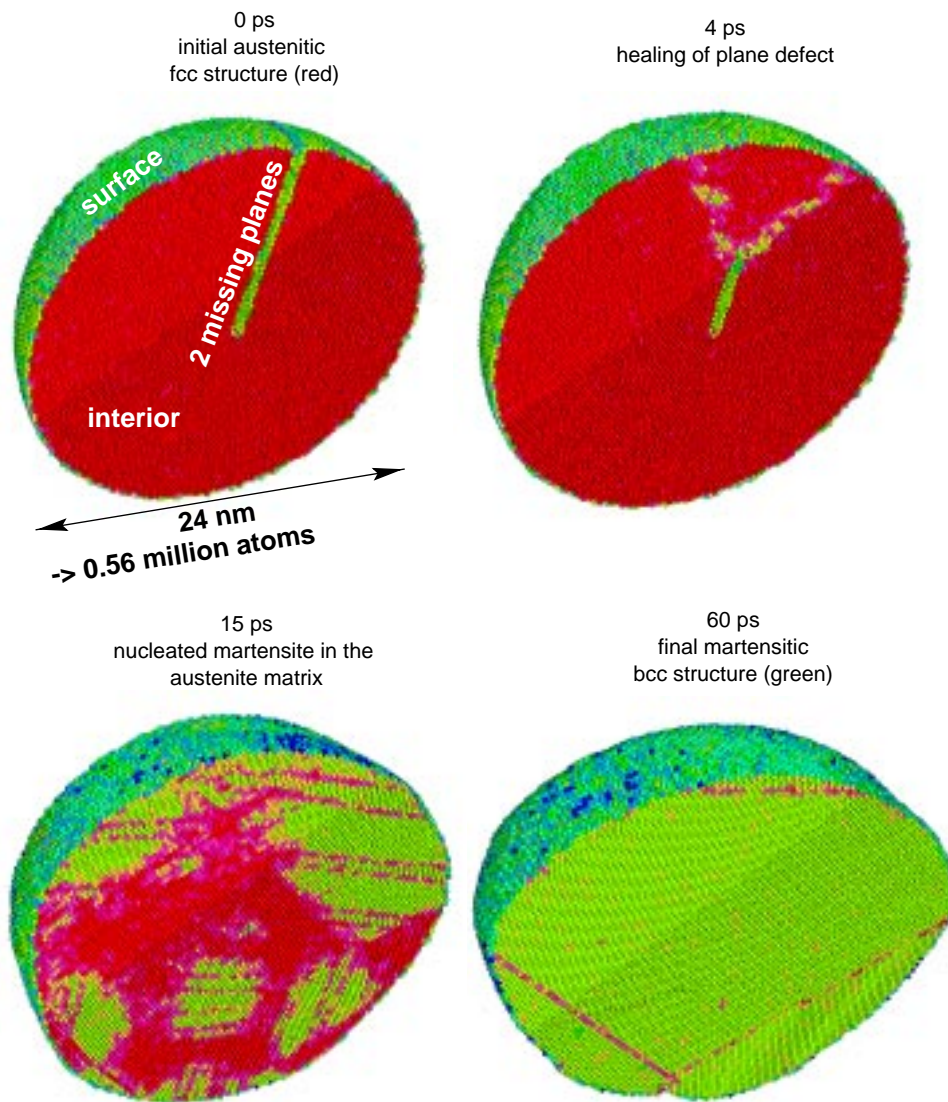


Figure 1: Heterogeneous martensitic nucleation at a plane defect in an otherwise ideal spherical $\text{Fe}_{80}\text{Ni}_{20}$ nanoparticle at 50 K. The intermediate structure obtained after 15 ps simulation time exhibits a pattern of differently oriented martensitic variants embedded in the austenite matrix.

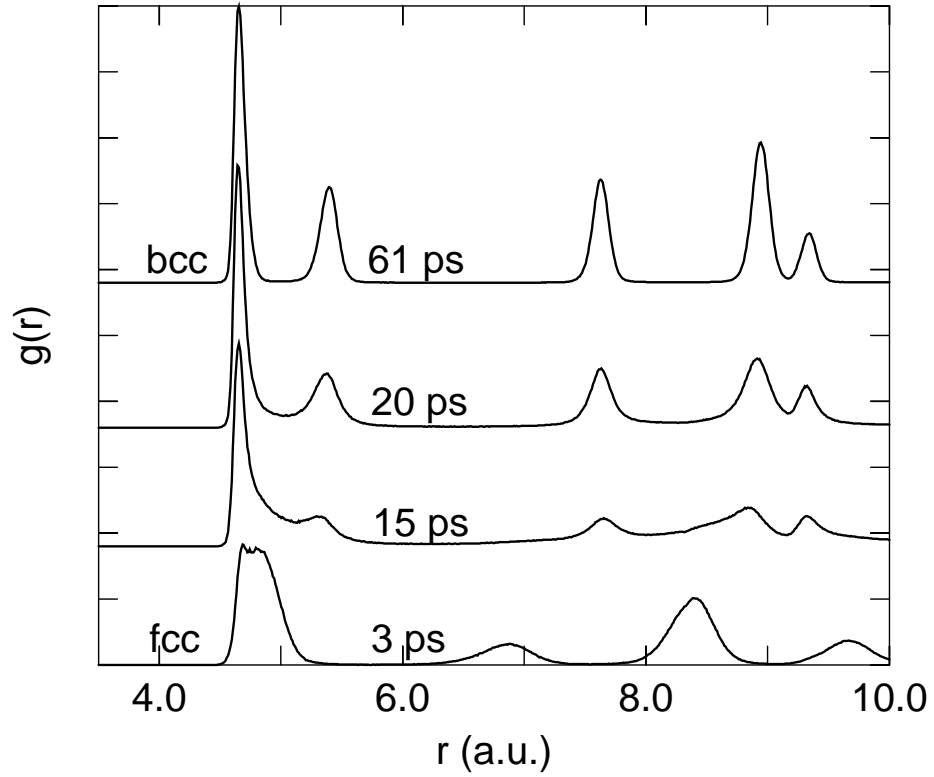


Figure 2: Time evolution of the radial distribution function of a spherical particle of $\text{Fe}_{80}\text{Ni}_{20}$ containing about half a million atoms. After the nucleation starts at the pre-existing plane defect shown in Fig. 1, the final transformation from fcc into bcc at $T = 50$ K leads to a splitting of the first neighbor peak of the fcc structure (12 nearest neighbors) into two nearest neighbor peaks of the bcc structure (8 nearest and 6 second nearest neighbors).

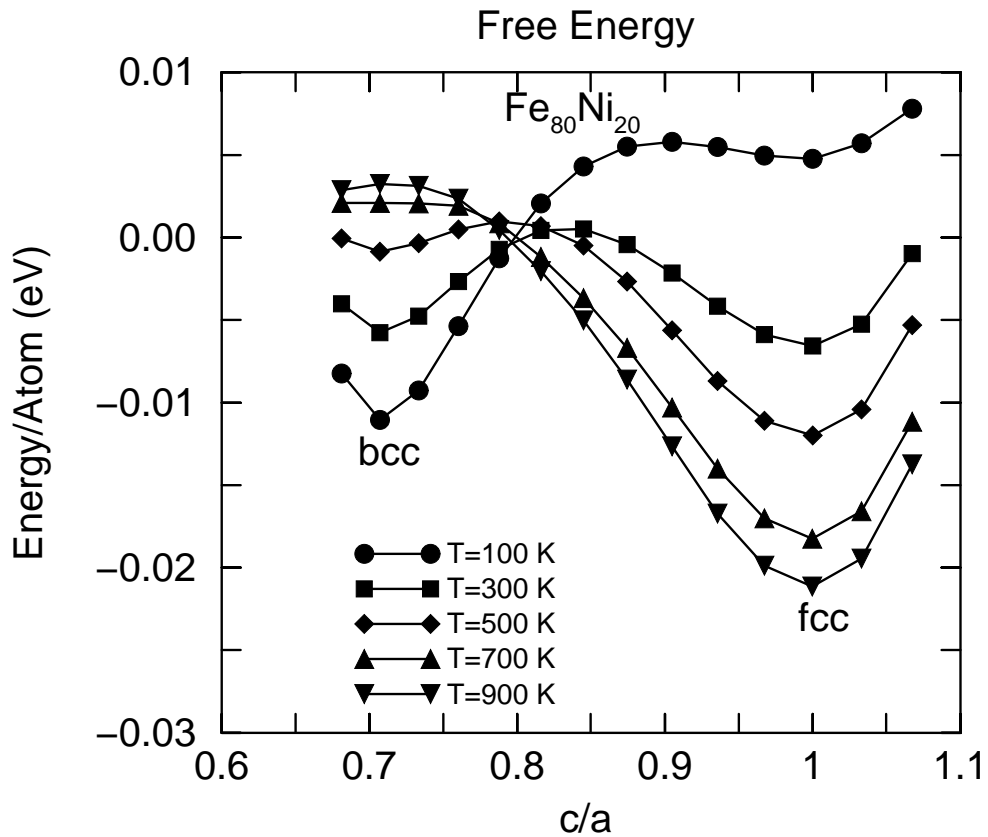


Figure 3: Behavior of the free energy along the Bain path for bulk $\text{Fe}_{80}\text{Ni}_{20}$ at different temperatures. The minimum in the free-energy curve of the bcc state vanishes at high temperatures where the fcc structure becomes stable. In contrast to this, there remains a minimum in the free-energy curve for the fcc structure at low temperatures (metastable fcc structure). The system has to overcome a small energy barrier in order to complete the martensitic transition from fcc to bcc with decreasing temperature.